International Journal of Communication Networks and Information Security
2024, 16(S1)
ISSN: 2073-607X, 2076-0930
https://https://ijcnis.org/ **Research Article**

Brain Tumor Segmentation and Classification Based on Deep Learning Using a Dense-Net Recurrent Neural Network

S. Syed Ibrahim[1*], Dr. G. Ravi[2]

[1*]Research Scholar PG & Research Dept. of Computer Science Jamal Mohamed College (Autonomous) (Affiliated to Bharathidasan University) Tiruchirappalli, Tamil Nadu, India.
[2]Associate Professor & Coordinator Department of Computer Science Jamal Mohamed College (Autonomous) (Affiliated to Bharathidasan University) Tiruchirappalli, Tamil Nadu, India.

Email: [2]ravi_govindaraman@yahoo.com
Corresponding Email: [1*]syedibs@gmail.com

ARTICLE INFO

Received: 04 May 2024
Accepted: 12 Sep 2024

ABSTRACT

Brain tumors are malignant cellular growths that spread uncontrollably throughout the brain. The subsequent prognosis and treatment planning depend heavily on the accuracy of tumor segmentation. For the purpose of segregating tumors, Deep learning brings into consideration of unidentified location of malignancies inside certain regions when analyzing Magnetic Resonance Imaging (MRI) data. To achieve adaptable and efficient brain tumor segmentation, it first presents a pre-processing technique that focuses on a restricted region of the image rather than the complete image. This technique is simple and efficient since it analyses only a small portion of the brain image in each slice during the second phase, thus reducing computing time and avoiding the over fitting problem that plagued previous deep learning models. For feature extraction, a Recurrent Softmax Convolutional Neural Network (RS-CNN) based on the Dense Net Recurrent Neuron Network (DNRNN) is proposed. In addition, the Fuzzy Clustering Scaled Network (FCSN) mechanism is introduced to enhance the segmentation accuracy of brain tumors over existing models. To measure the performance, a Dense Net Recurrent Neural Network (DNRNN) is utilised to construct feature maps that modify the core network and classify the ensuing feature maps. These feature maps are then used to generate tumor area charts with prediction accuracy. The suggested method was evaluated on MRI brain images with malignancies using the Unique Client identification (UCI) data set. The results showed that the test time improvement enhanced the tumor segmentation accuracy.

Keywords: Deep Learning, Magnetic Resonance Imaging (MRI), Fuzzy Clustering Scaled Network (FCSN), Brain Segmentation, Brain Tumors.

INTRODUCTION

The brain, which is widely regarded as the body's most crucial organ, is susceptible to the fatal disease known as brain cancer, which claims the existence of a large number of people. Brain tumor cells multiply uncontrollably and eventually consume nearly all the nutrients intended for healthy cells and tissues. Early diagnosis of brain tumors is now possible because of an easily accessible technology for their detection and categorization [1]. Several image processing approaches, such as image segmentation, image enhancement, and feature extraction, have been developed for the diagnosis of brain tumours based on MRI of cancer patients. Currently, physicians determine the location and extent of the brain tumor by manually examining Magnetic Resonance Images of the patient's brain. This results in imprecise tumor detection and is considered a time-consuming process. In clinical diagnostics, cancer segmentation constitutes the most significant challenge. This work focuses on a system that employs computer-based procedures to detect tumor blocks and segment the tumor using a Convolution Neural Network Algorithm for MRI of various patients [2]. To detect a brain tumour using Image Processing methods, four steps must be taken: image pre-processing, image segmentation, feature extraction, and classification. Figure 1 depicts the use of image processing and neural network techniques to enhance the performance of detecting and classifying brain tumors in Magnetic Resonance Images.

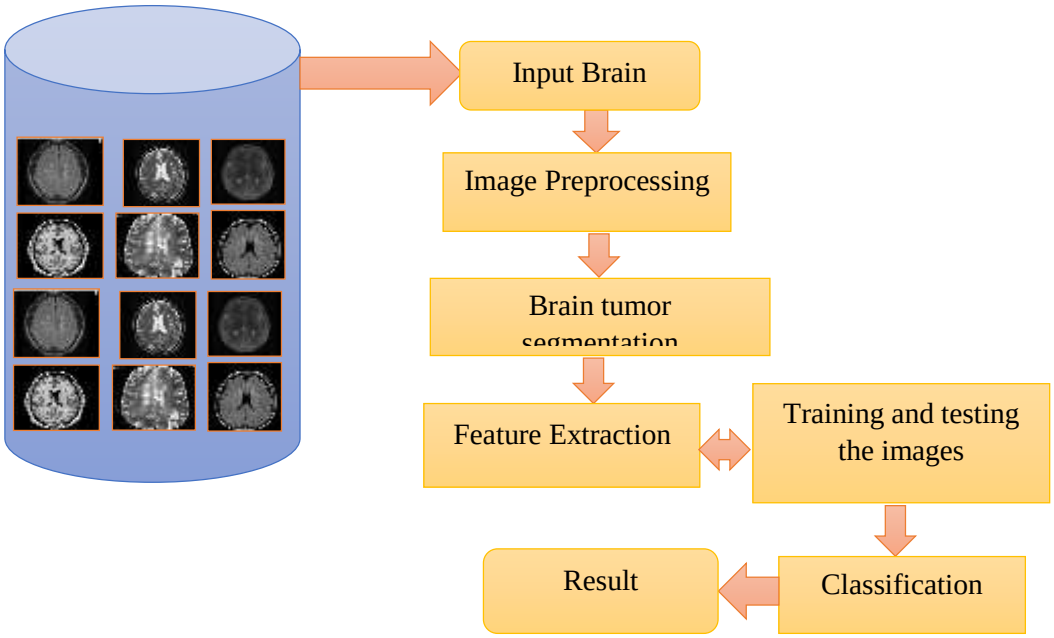

Figure 1: Basic Flow diagram

Recurrent Softmax Convolutional Neural Network (RS-CNN) architecture with Visual Geometry Group -16 uses a patch-based strategy to predict output labels. This method considers both local and empirical data. [3]. The network addresses the issue of varying definitions by integrating dropout regularisation and the compound training technique. This work presents about deep learning-based technique for brain tumor segmentation using multiple Magnetic Resonance Imaging modalities.

LITERATURE SURVEY

It has become a well-known fact that the brain is considered as the most essential organ in the human body. Considering the complex nature of brain structure, prediction of the cancer tissues can take a significant amount of time. In addition, there is a need for specialists with the skills can able to examine the images to recognise the impacts. In this view, due to the high mortality rate of brain tumors, it is necessary to detect the disease in its primary stages as early as possible. Nevertheless, brain cancer is an incurable disease that results in the loss of existence for a large number of people. The unchecked and fast proliferation of cells can lead to the development of brain tumors. Accurate segmentation and classification is still a difficult problem, despite the numerous substantial efforts that have been made and the encouraging results that have been obtained in this field. The purpose of the study was to conduct a comprehensive literature review of MRI for the diagnosis of brain tumors.

S. Banerjee et al, suggested that medical imaging data from a large number of patients is becoming increasingly accessible. The author introduces an innovative technique for automatic, accurate, and reliable 3D segmentation of tumors using MR images acquired in several sequences. When this is applied to the BRATS dataset, the proposed segmentation method is shown to be highly accurate, reliable, and resilient which contains visual data of intricate details from photos of many types [4].

Rehman et al, suggested the deep learning technique for detecting and classifying tumors in brain. First, tumors are extracted using a 3D convolutional neural network architecture, with the resulting data being fed into a relevant CNN model for feature extraction. In the correlation-based selection process, the retrieved features are used to make a final decision. For the ultimate classification, these chosen characteristics are verified using a feed-forward neural network [5].

An Hu and Navid Razmjooy uses a new metaheuristic-based system using a deep belief network. to provide a technique for early detection of brain tumors. To choose characteristics and categorise photos optimally, a modified version of the seagull optimisation method is used [6].

T. Saba et al, present the Grab cut method for segmentation correction. Moreover, features are acquired using a fine-tuned version of the transfer learning model Visual Geometry Group (VGG-19), which are then serially combined with features that were manually constructed (shape and texture). To maximise classification accuracy and speed, entropy is applied to these features, and the resulting fused vector is sent to classifiers [7].

P. Kaur et al initiate the initial phase of segmentation, which divides the tumor into benign and malignant parts using filtering methods that are accessible in image processing, the next step is classification, which will be carried out once the segmentation has been completed. Finally, a multi-support vector method, capable of detecting the tumor in MRI images, is used to evaluate the effectiveness of the suggested techniques [8].

T. Pandiselvi and R. Maheswaran introduce an innovative technique known as the Adaptive Convex Region Contour (ACRC) algorithm which provides an efficient segmentation by making use of MRI slices, that can assist in locating the tumor along with its true dimensions and contours. A Support Vector Machine is used to categorise a segment either

healthy or unhealthy. After getting the results of the SVM, the aberrant slices will be incorporated into the segmentation process [9].

T. Zhou et al provide a correlation model that has been created to specifically depict the latent multi-source correlation as a result of the fact that there is a high connection that occurs between several modalities. This correlation representation represents the segmentation became more reliable in the event when a modality was absent. First, an estimate of the parameter that is independent of the encoding mode is derived from the individual representation that is created by each encoder. The separate representations are then converted into latent multi-source correlation representations via the correlation model [10].

Guotai Wang et al suggested a series of Convolutional Neural Networks (CNNs) that divides brain tumors into hierarchical sub-regions based on multi-modal MRI. The author also use test-time enhancement to improve the accuracy of segmentation. This gives us information about the uncertainty of the segmentation result at the voxel and structure levels [11].

Dingwen Zhang et al propose an entirely new structure that will permit deep learning with the intent of categorizing brain tumors based on many modalities of MRI data. The primary objective is to detect patterns within the multi-modality data in order to make up for the inadequate in the amount of individual data points. The framework for deep feature learning for cross-modal data that was suggested to utilizes two different learning algorithms, namely: CMFT and CMFF which includes acquiring rich feature representations by transferring knowledge between modalities and combining modalities' knowledge [12].
Zhengrong Luo et al suggest that for quick and accurate segment 3D volumetric images, the author uses a Hierarchical Decoupling Convolution Network, a lightweight yet effective pseudo-3D model. In this work, the author replaces traditional 3D convolutions with Hierarchical Decoupled Convolution module that efficiently probes spatial contexts at several scales and perspectives. Extensive testing on the BraTS 2018 and 2017 datasets has shown that the approach is more accurate than the newest available technology while dramatically reducing computer complexity [13].

A. Gumaei et al, present a classification strategy for brain tumor where the author uses a Regularised Extreme Learning Machine to extract hybrid features. A hybrid feature extraction method collects brain tumour features after min-max normalisation improves brain edge contrast. A new public brain scan dataset is used to test and compare the proposed approach [14].

Dingwen Zhang et al recommended that the first feature is called task-modality structure and the second feature is called task-task structure. Here, the author presents a novel task-structured brain tumor segmentation network. To investigate this task-modality structure, the researcher developed a modality-aware feature embedding method that employs network learning to determine the data weights for each modality. To investigate the task-task structure, the authors conceptualise tumor area prediction as subtasks with conditional dependence and embed this dependence within the network stream. [15].

G. Manogaran et al, employ an enhanced machine-learning approach based on the orthogonal gamma distribution to analyse the under-segmented and over-segmented regions of brain tumor areas, aiming to detect abnormalities through automatic region of

interest (ROI) detection. When the edge coordinates are matched, it eliminates the data imbalance that occurred during sampling in the abnormality zone and allows for an evaluation of the sensitivity and selectivity parameters through a machine learning algorithm [16].

M. S. Majib et al propose 16 different models for transfer learning that were considered for the purpose of determining the most effective option for neural network brain tumor classification. To categorise brain cancer images of human interaction, different conventional and hybrid machine learning representations were constructed and rigorously analysed to classify brain cancer images without human intervention [17].
Y. Zhuang et al, recommend that MR images are segmented using an ACMINet (Aligned Cross-Modality Interaction Network) to identify brain tumor and tissue areas. The cross-modality feature interaction module of this network was initially created to effectively and adaptively combine and modify multi-modal features [18].
M. A. Ottom et al introduce Znet Framework, which improves brain tumor cell detection and anatomical structure analysis by training and classifying data in neural network systems and tumor cell segmentation using AN & Unet approach. The TCGA-LGG compilation's objective is to develop cancer images for research purposes in addition to investigating the relationship between phenotype and genotype in cancer and medical image research [19].
Y. Ding et al provide complementary-view characteristics, it is recommended that a hierarchical multi-view convolution strategy be created. The standard three-dimensional convolution should be uncoupled into axial, coronal, and sagittal planes using this procedure. The author suggested that the structure is made up of three major construction parts. To begin, a multi-view deep neural network architecture comprises numerous learning networks for segmenting the brain tumor from various perspectives. The dynamic decision fusion strategy integrates segmentation data from several perspectives utilising voting and weighted averages to evaluate the fusing process. Finally, the multi-view fusion loss (composed of segmentation loss, transition loss, and decision loss) simplifies multi-view learning network training by ensuring constancy in form and position between segmentation results and learning network training [20].

K. Muhammad et al include the essential processes of deep learning-based Brain Tumor Classification (BTC) for example Pre-processing, feature extraction, and Classification, as well as their successes and shortcomings. This paper compares sophisticated Brain Tumour Classification with and without data augmentation using convolutional neural network models. This summary also provides an overview of the benchmark data sets that are currently available for analysing BTC [21].

M. Ali et al, propose a 3D CNN and U-Net are ensembles of two segmental networks. A better and more accurate prediction results in a remarkable and straightforward compounding technique. Automated segmentation is one of the most important multimodal MR images of brain tumor for the analysis and monitoring of disease progression [22].

T. A. Soomro et al, propose advancements and efficient computing that enable in machine learning a computer-aided solution to analyse MRI images and effectively detect abnormalities promptly. Medical image analysis has become a hot and research-intensive area in the community. However, this is considered a time-consuming and labor-intensive process [23].

MATERIALS AND METHOD

When MRI scan is considered as the primary input its efficacy is determined by the accuracy of the given predictions. Data processing techniques such as thresholding and error correction were applied to reduce the amount of background noise in the MRI images that were used to evaluate the level of performance. Using Dense Net Recurrent Neuron Network (DNRNN) technology, an automatic brain tumor detection and classification system is constructed. The VGG16 framework is used by the Recurrent Soft-max Convolutional Neural Network (RS-CNN) to build feature maps that transform into core networks and classify these feature charts to generate tumor regions.

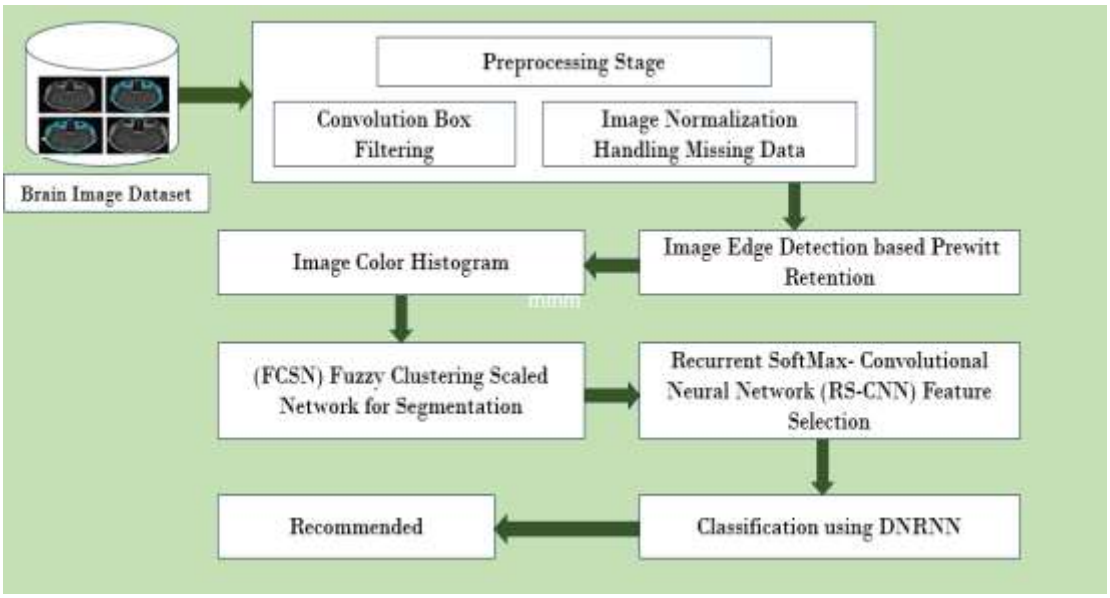

Figure 2: Proposed Block diagram

Figure 2, Dense Net Recursive Neuron Network (DNRNN) begins with the process of Convolution Box filtering is used to smooth an image. Linear filtration operates by restoring neighborhood pixels in a liner mix fashion. It enhances the image by sharpening the edges and redressing the illumination, resulting in a standard image. Prewitt Retention log-based image edge detection is used to detect the appearance of brain imaging features and to cover their exact boundary areas to segment them. Image Colour Histogram (ICH) is split up into brain regions to provide scaled weights for feature levels. After that, a Fuzzy Clustering Scaled Network (FCSN) is used for image segmentation to slice each image according to its respective weights. It is easier to differentiate between tumor and non-tumor classes, the selected characteristics are put through training and evaluation with the DNRNN classification. As a result, performance is enhanced, and existing systems are used to provide additional support for recommending categorization outcomes.

3.1 Image Preprocessing Using Convolution Box Filtering

The process of convolution is an important aspect in linear filtering, that is used to smooth an image. Linear filtration operates by restoring neighborhood pixels in a liner mix fashion. It enhances the image by sharpening the edges and redressing the illumination, resulting in a standard image. The following algorithm describes the process for creating a binary window around a pixel in an image based on a certain distance measure and threshold. The neighborhood pixels are defined by the binary window.

Given a binary window w of side 'w_S', a distance measure 'd', a pixel p(x, y) at coordinates x and y belonging to an image of size m x n, & a threshold t:
if ($w_S/2 < x < (m + 1 - w_S/2)$ and $w_S/2 < y < (n + 1 - w_S/2)$)
begin:
For i = 0...w_S do
For j = 0...w_S do
if ($d(p(x\ [\frac{w_s}{2}]+i,\ y - [\frac{w_s}{2}] + j),\ p(x, y)) \leq t$)
w(i, j) = 1
else w(i, j) = 0
$w = \frac{w}{\text{total (where w=1)}}$
Return w

3.1.1 Handling Missing Data

Missing data imputation occurs naturally as part of the Machine Learning (ML) estimation of the Convolution Box filtering parameters, which considers two independent submatrices: o X, which contains the observed data, and m X, which contains the missing data. The E-step of the E-M algorithm computes the expected complete log-likelihood.

$$L_o\,(W, \beta, v|X^o, X^m, Z) = \sum_{n=1}^{N}\sum_{k=1}^{K} z_{kn}\ \log|C_k\left[1 + {}^{\beta}/_{V_k}\,(\|y_k^o - x_n^o\|^2 + \|y_k^m - x_n^m\|^2)\right]^{\frac{V_k+D}{2}} \quad \text{Eq. (1)}$$

Where Ck is a summary coefficient and Z is an indicator matrix, with elements kn, z representing our ignorance of which latent point k, u is responsible for data point nx creation. The necessary statistics must be computed.

3.2 Image Edge Detection-Based Prewitt Retention Log

There are just two horizontal and two vertical templates available in the classic Prewitt edge detection operator. Since edges can occur in several directions, an operator with eight direction-specific templates is proposed, increasing the number of edges that can be detected. At this point, the entire Tumor region is divided into movable windows. This resulted in a reduction in the number of pixels with correlated edges in the scaled upper-bound region. Sliding the arch corner curves finds weights at the corners to choose edge locations, allowing log retention to be used to detect a growing state at each edge point. In order to process the grayscale image, the retention maps the image's corner boundaries to create the space log events.

$$m_{pq} = y^q\, f(x, y)dxdy \quad \text{Eq. (2)}$$

This equation gives us the formula for the order centric distance.

$$u_{pq} = (y - \bar{y})^q f(x, y)dxdy \quad \text{Eq. (3)}$$

Where y and $\bar{y}$ is an image fusion metric that defines the edges, these edges are determined by the classification edge points. The classified central point's corrective edges need to be changed at the level to achieve the desired result. A differential third order equation must be used, and f (x, y) generates 0's and 1's for variant and invariant edge points.

$$(\text{Size } 1) = S + \eta_{02} \quad \text{Eq. (4)}$$

$$(\text{Size } 2) = (\eta_S - \eta_{02})^2 + 4\eta_{s11}^2 \quad \text{Eq. (5)}$$

Take the square of the formalized level to determine that both values are of the first order of linear obviation.

$$(\text{size } 3) = \log(\eta S_{30} - 3\eta s_{12})^2 + (\eta s_{21} - \eta_{s03})^2 \quad \text{Eq. (6)}$$

$$(\text{size } 4) = \log(\eta s_{30} + 3\eta s_{12})^2 + (\eta s_{21} + \eta s_{03})^2 \quad \text{Eq. (7)}$$

Subspace entities between linear data are generated by logarithmic differentials due to differences in variance. To acquire the robust weights, this allows for the maximum corner x, and edge points at x_{max} to be supported based on the log retention concept. This maximizes tumor feature enhancement within the normalized 0.3 mm scaled metric range up to the crossover maximum edges.

3.3 Color Histogram Images

Histograms are graphical representations that illustrate the frequency with which different color values appear in an image. A color histogram is a depiction of the distribution of colors inside an image that is used in image processing. It is a representation of the number of pixels in an image that includes colors that fall within each of a predefined set of color ranges. The color dependencies of the histogram were scaled according to the degree of tumor depending on the color channel. Additionally, to gain a scaled entity, the projection tumor level must first obtain the regular body of the object. This is a prerequisite for receiving a scaled entity. To standardize the intensity of the backing, each characteristic has been evaluated using the canonical method, and the static features are histogram features. As a result, the highly scattered image moves closer and closer to a single point where the probability index may be obtained, allowing the tumor level of the covered pixel to be located.

$$H(s) = H(s)/N \qquad \text{Eq. (8)}$$

It chooses the image where the grey levels form high intensity with brightness and an increased mean rate to establish the Low contrasting 'L' at grey range from 0 to 1 at the standard point to make the average brightness.

$$\breve{g} = \sum_{g=0}^{L-1} gP(g) = \sum_{g} \sum_{g} \frac{I(r,c)}{M} \qquad \text{Eq. (9)}$$

In the tumor level's pixelated representation, Rows and columns where the variance of a constant equation deviates from the low-contrast pixels are represented by the present supporting 'g' points. As the square root of the sum of the pixels, this improves the tumor level pointing.

$$\sigma_g = \sqrt{\sum_{g=0}^{L-1} (g - \bar{g})^2 P(g)} \qquad \text{Eq. (10)}$$

According to the tumor level point of entity covered object, To determine whether or not two pixels are statistically close together, their histogram spreading ratios must be compared using a curved region whose intensity levels are equal [24].

3.4 Fuzzy Clustering Scaled Network (FCSN) for Segmentation

When working with color images, it might be challenging to analyze the whole image based on all of its colors. It has been possible to organise probable colors through the use of soft computing techniques which is the process of extracting individual colors from a given image by utilising fuzzy clustering methods and a competitive neural network. The act of splitting the pixels in an image into distinct groups or clusters is known as image segmentation. The most essential characteristics for image segmentation are the luminance amplitude in the case of a black-and-white image and the color components in the case of a color image. Image segmentation is used to group colors that are likely to appear together in an image. This is necessary since there are more than 16 million colors that may be shown in any one image, and it is impossible to evaluate the image based on all of its colors. This is done so that the objects in each class are as comparable to one another as is feasible, while the things in other classes are as unlike one another as is possible. The tumorous images were processed in such a way that malignancy areas could be removed from them.

Tumor segmentation is a challenging and time-consuming operation due to the intricate nature of the brain.

The difficulty in the segmentation task is exacerbated by the low contrast and correlated MR data. It is necessary to segment the section of the image that contains the tumor to get the data ready for the next step of the classification process, which will determine the type of tumor, its size, and its location. Segmentation in an MR image of the brain is already a challenging task due to the overlapping tissues and layers present in the image. This complicates matters even further.

$$y_p = \frac{\sum_{p=1}^{c} u_{ip}^{q} \sum_{j=i-2}^{i+2} x_j/5}{\sum_{p=1}^{c} u_{ip}^{q}} \qquad \text{Eq. (11)}$$

where u_{ip} indicates the membership value of pixel i in class p. Averaging the two images before and after the current one gives an improved view of the scene than utilizing a single image's intensity value at point i where the Image intensity is xj. The total number of classes.

$$\partial f(a,b)\,\partial b = \lim \Delta \to 0 f(a, b+\Delta) - f(a,b)\Delta \approx X[i, j+1] - X[i,j] = H[i,j] \qquad \text{Eq. (12)}$$

A directional variation in intensity or color inside an image can be quantified using something called an image gradient. When it comes to image processing, the most important element of structure is the gradient of the image. The phrase "gradient" or "color gradient" is also used to refer to a progressive combination of colors, which can be conceptualized as a gradient from low to high values. Image processing is one of the most important fields of study in the field of computer science. Color progression is yet another name for this phenomenon. The gradient of an image can be computed; The average can be used to compute the intensity variation of each pixel, which can then be approximated using partial derivatives.

$$\frac{\partial f(a,b)}{\partial a} = \lim_{\Delta \to 0} \frac{f(a+\Delta,b) - f(a,b)}{\Delta} \approx X\{i+1, j] - X[I, j] = V[I, j] \qquad \text{Eq. (13)}$$

After producing the gradients for all 32 photos (using characteristics retrieved from the most recent convolution layer), Instead of using a matrix of form (32,32,32), which would have been necessary to get the individual relevant measurements, they computed their average and global maximum and combined them into two vectors of size 32

$$q'_x = \arg\max_{L \epsilon \{L_1, L_2\}} \sum_{p_k \epsilon \alpha(p_x)} F(q_x = L) \qquad \text{Eq. (14)}$$

$$q'_x = \max\left\{\sum_{p_k \epsilon \alpha(p_x)} F(q_x = L_1) \sum_{p_k \epsilon \alpha(p_x)} F(q_x = L_2)\right\} \qquad \text{Eq. (15)}$$

Where L1 and L2 are the classification labels, q ′ x is the predicted label, F() is a representation of the function values that can be either 1 or 0 depending on the true/false condition, and (px) denotes the closest neighbors. The FCM algorithm must decrease the Fm value dependent on the number of iterations. The following equation for updating provides the necessary condition for minimizing, which is shown below.

$$a_i = \frac{\sum_{j=1}^{n} (\mu_{ij})^{m} y_j}{\sum_{j=1}^{n} \mu_{ij}^{m}} \qquad \text{Eq. (16)}$$

$$\mu_{ij} = \frac{\|y_j - a_i\|^{\frac{-2}{m-1}}}{\sum_{k=1}^{c} \|y_j - a_k\|^{\frac{-2}{m-1}}} \qquad \text{Eq. (17)}$$

The fuzzy clustering algorithm is the one that gets the most applications. This FCSN technique, on the other hand, requires a significant amount of computational effort and is sensitive to the beginning speed, local minima, and low membership degree for noisy spots. The FCSN protocol is implemented as a solution to the issue. The FCSN approach makes use of clustering, which has the potential to eradicate noise and corruption in big data sets.

1. Write k as the value for the number of clusters.
2. Select at random the k locations where the clusters are concentrated
3. Determine the cluster's mean or the geographic centre of the cluster.
4. Determine the distance in pixels between each pixel and the centre of each cluster.
5. If the distance to the canter is rather close, you should proceed to that cluster.
6. If this is not the case, proceed to the next cluster.
7. Perform a new calculation for the centre.
8. Carry on with the method until there is no longer any movement in the centre

In addition to defining the information that is present in an image, the membership function is responsible for determining how fuzzy an image is. These are the three most important fundamental features that are involved in determining membership function. They are there to help, Boundary. The core participates in every aspect of the fuzzy set. The support is the value of the set that indicates that the individual is not a member of the set, and the boundary indicates intermediate or partial membership with a value between 0 and 1. The clustering technique known as FCSN is the one that enables a single data point to participate in more than one cluster simultaneously. It achieves this by decreasing the function that is shown below:

$$y_m = \sum_{i=1}^{N}\sum_{j=1}^{C} M_{ij}{}^{m} \left\|x_i - C_j\right\| \quad \text{Eq. (18)}$$

Where m is any real number bigger than 1, Mij x is the degree of membership of X, and j, i Rj is the d-dimensional core of the cluster. - data measured in d-dimensional, The latest information about the members of MIJ and the centres of clustering.

3.5 Selecting the Images Based On Recurrent Softmax Convolutional Neural Network (RS-CNN) Feature Selection

When more resources become available, Relation Shape Convolution Neural Network architectures can grow further, leading to improved performance through scaling. Traditional methods of model scaling have involved adjusting the Relation Shape Convolution Neural Networks in depth. Although this technique has the potential to increase performance in circumstances in which it has been trained to use RS-CNN architecture, manually integrating these components can be challenging. In the Deep learning (DL) model's convolution layer, the acquired kernels from the previous layer's in-depth features are used to construct the throughput feature map. Multiple maps are used as input to a convolution that can provide a single output map. Weights are used for learning both spatial and high-level qualities.

$$\square_p^q = R\left(\beta_p^q + \sum_{r=1}^{N^{q-1}} \omega_{p,r}^q \, x M_r^{q-1}\right) \quad \text{Eq. (19)}$$

Where, $\delta_p{}^q$ indicates layer output, bias represented as $\beta_p{}^q$ represents bias, $w^q{}_{p,r}$ represents the layer weight and $M_r{}^{q-1}$ represents the layer inputs which is used as the activation function. The weights can be fine-tuned by feeding the output of one layer into the input of the next layer.

$$R(M) = \max(0, M) \quad \text{Eq. (20)}$$

$$\square_p^q(\max) = \text{Pool}_{\max} \text{Rel}(M)), \text{Rel}(M) \epsilon \square_p^q \quad \text{Eq. (21)}$$

The stride value is used to translate all matrices in a layer whose characteristics are the filter dimensions. The activation function is represented by the notation softmax f(s)i.

The loop procedure to choose the best inputs for optimization classifier

i = 1,

n = total number of attributes,

attribute(i) represents the rank i attribute in the importance list generated

by neural networks algorithm.

Repeat

select attribute (1) to attribute(i) as input attributes to build classifier
calculate the error rate → e(i)
i++
Until in or e(i)> e(i-1)
Output: the optimization classifier model with i attributes
The main goal of this study is to use the neural network model to find the best weights to lower the difference between input and output performance metrics. It represented in a neural network method, each input variable's relevance is quantified by assigning a numeric value between 0 and 1 to its chromosomes, with higher numeric values corresponding to more significant inputs. The estimated relative importance of each variable in the model's performance was calculated using a sensitivity analysis of the neural network.

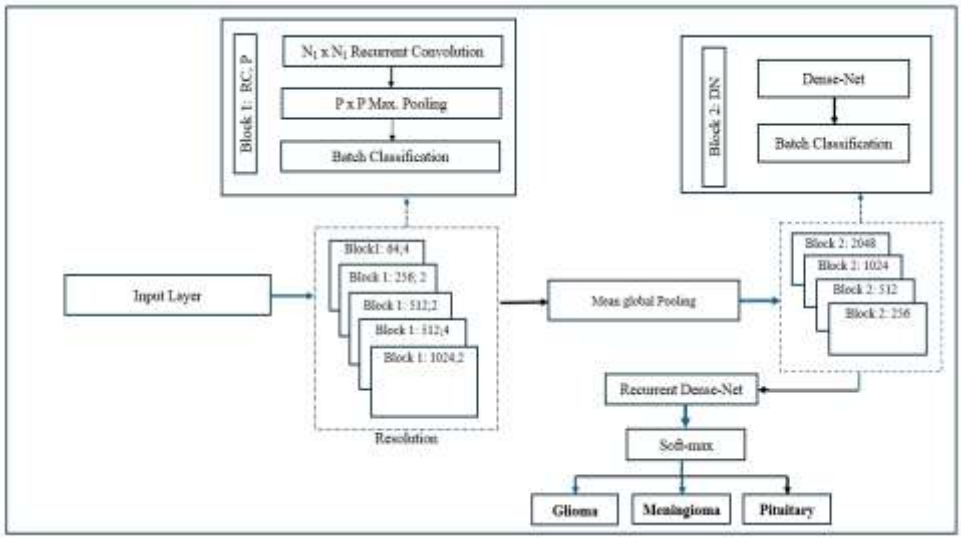

Figure 3: Feature selection using RS-CNN Layers

Meningioma, glioma, and pituitary tumor classifications were all accomplished using the proposed feature selection "25-layers RS-CNN" architecture. Figure 3 depicts the suggested architecture in action, it receives MRI slices as input, processes those slices in layers, and ultimately distinguishes between them.

3.6 Classification Using DNRNN

When compared to other neural networks, DNRNNs have a significantly greater number of layers. Pattern recognition and image processing both stand to gain considerably from the application of this effective recognition method. By using a shared-weight network structure, it mimics the functioning of a biological brain network. The DNRNN model consists of a series of convolution and pooling processes, followed by a fully connected layer. The characteristics that are derived from the DNRNN which have a quality that is generally perpetual. Softmax is used in the final output layer because it may be used for multiclass classification.

LoadImage();
dataAugmentation();
splitData();
loadModel();
for each epoch in epochNumber do
for each batch in batchSize do
 $\hat{y}$ = model(features);

loss crossEntropy (y, ŷ);
optimization(loss);
accuracy();
best Accuracy = max(best Accuracy, accuracy);
return
The model may be constructed by using the Adam optimizer and binary cross-entropy as a loss function, and determined its accuracy in tumor detection.

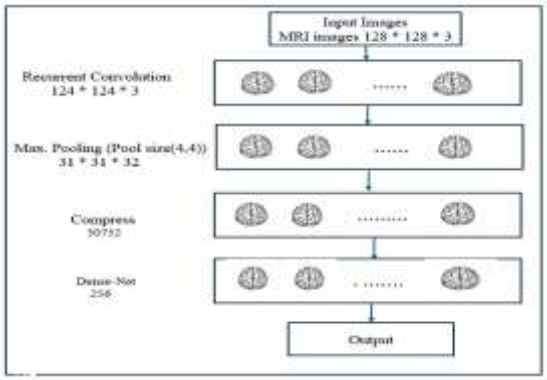

Figure 4 Recurrent Convolutional Neutral Network

The MRI images are transformed into a uniform 64x64x3 pixel resolution by using a convolutional layer as the first learning layer. As it may be used to the convolutional kernel may use to convolute the input layer by utilising 32 convolutional filters of size 3x3 each with the aid of 3 channel tensors, after collecting all the images in the same orientation. As an activation function, ReLU is utilized to ensure that the results do not match up with those shown in Figure 4.

RESULT AND DISCUSSION

This section illustrates the different performance metrics used to evaluate the proposed method for the segmentation and classification of brain tumor. The environmental setup is depicted in the following table.

Table 1: Environmental Setup

Simulator language	Python
Simulator Tool	Anaconda
Dataset name	MRI brain tumor
Number of images	500

This paper uses MRI brain tumor images collected from the online Kaggle repository. It has two folders with brain and without brain tumors containing 500 MRI brain images. This dataset includes 305 MR brain images in a folder with a brain tumor and a folder without a brain tumor containing 195 MRI brain images. The performance of the proposed system is analyzed in terms of specificity, sensitivity, accuracy, and False Score by the following equations.

$$\text{Specificity}=\sum \frac{T_n}{F_p+T_n} * 100 \qquad \text{Eq. (22)}$$

$$\text{Sensitivity} =\sum \frac{T_p}{T_p+F_n} * 100 \qquad \text{Eq. (23)}$$

$$\text{Accuracy}=\sum \frac{T_p+T_n}{T_p+F_n+F_p+T_n} * 100 \quad \text{Eq. (24)}$$

$$\text{False Score} = \sum \frac{F_n+F_p}{T_p+F_n+F_p+T_n} * 100 \quad \text{Eq. (25)}$$

True Positive (TP) – predicts the positive class (e.g. disease confirmed)
True Negative (TN) - predicts the negative class (e.g. no disease)
False Positive (FP) – incorrectly predicts the positive class (e.g. no diseases)
False Negative (FN) – incorrectly predicts the negative class (e.g. disease)
These are to be evaluated by comparing the Predicted Image (PI) and Ground Truth image (GTI) that are defined below
True Positive (TP): the pixel value of GTI and PI has one
False Negative (FN): it provides a pixel value of GTI as one and the pixel value of PI is zero.
False Positive (FP): it provides a pixel value of GTI as zero and the pixel value of PI is one.
True Negative (TN): the pixel value of GTI and PI is zero.
The pixel values of both GTI and PI evaluations are used to calculate the value of specificity, sensitivity, Accuracy, and False Score values.
The proposed Dense-Net Recurrent Neuron Network (DNRNN) is going to be tested with metrics such as Specificity, Sensitivity, Accuracy, False Score, and these metrics are compared with other methods like Generative Adversarial Network (GAN), Hierarchical Decoupled Convolution Network (HDC-Net), Diffusion-Convolutional Neural Networks (DCNN), Deep Belief Convolution Neural Classifier (DBCNC), Recursive Sigmoid Neural Network based on Multi-Scale Neural Segmentation (RSN^2-MSNS) which are calculated using images in terms of 100, 200, 300, 400, and 500 respectively and the graphical representation are plotted based on the given input.

4.1 Specificity

The Specificity is determined by taking the ratio of the percentage of accurately classified positive samples to the total number of samples that were determined to be positive in some way, whether correctly or wrongly.

Table 2. Comparison of Specificity (%)

No. of Images	GAN	HDC-Net	DCNN	DBCNC	RSN^2-MSNS	DNRNN
100	67	71	77	82	84	85.2
200	74	77	81	85	87	88
300	78	81	84	88	90	91
400	81	85	88	92	93	94
500	85	89	92	93.2	95	96

The collection of Brain images used to evaluate the proposed system which are compared with other methods is outlined in Table 1. The graphical representation of Precision in terms of percentage is shown in figure 5. The high values tabulated in Table 1 indicates that the proposed DNRNN scheme has high Precision values.

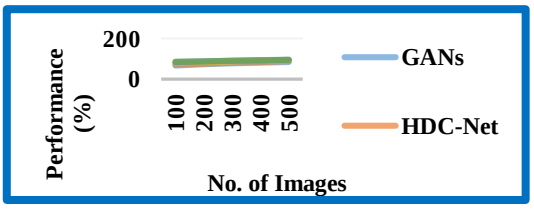

Figure 5: Comparison Chart of Specificity

Table 2 and figure 5, With 100 images, DNRNN specificity is 85.2% compared to RSN^2-MSNS specificity is 82%. With 500 images, DNRNN specificity is 96%, while RSN^2-MSNS reaches 95% specificity. The specificity gap between DNRNN and existing methods widens as more training data is utilized. DNRNN achieves the highest specificity, with 1-3% improvement compared to the next best-performing RSN^2-MSNS with datasets ranging from 100 to 500.

4.2 Sensitivity

The metric sensitivity is determining the proportion of positive samples that were positive compared to the overall number of positive samples. This ratio is then multiplied by 100. A measurement of the accuracy with which the model can identify positive samples is referred to as the recall.

Table 3. Comparison of Sensitivity (%)

No. of Images	GAN	HDC-Net	DCNN	DBCNC	RSN^2-MSNS	DNRNN
100	68	72	78	83	84	85
200	75	78	82	86	88	89
300	79	82	85	89	90	91
400	82	86	89	93	94	95
500	85	87	91	95	96	96.5

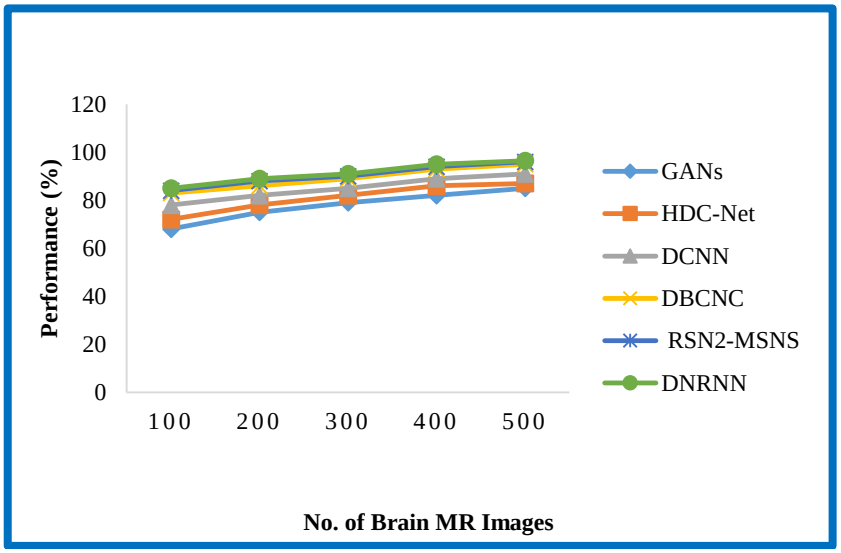

Figure 6: Comparison Chart for Sensitivity

Table 3 and figure 6 present the DNRNN method which consistently achieves superior sensitivity compared to GAN, HDC-Net, DCNN, DBCNC, and RSN^2 -MSNS indicating it as better and correctly identifying positive cases. DNRNN demonstrates better sensitivity and classification accuracy overall, compared to DCNN and the existing methods on the provided data. DNRNN achieves the highest sensitivity, with 0.5-1.8% improvement compared to the next best-performing RSN^2-MSNS with datasets ranging from 100 to 500.

4.3 Accuracy

Accuracy is a statistic that is used to represent, in a broad sense, how well the model performs across all different classes. When all of the classes are of the same significance,

it might be advantageous. It is determined by determining the ratio of the number of accurate forecasts to the total number of predictions that were made.

No. of Images	GAN	HDC-Net	DCNN	DBCNC	RSN2-MSNS	DNRNN
100	50	55	60	65	70	75
200	57	62	68	73	79	82
300	66	75	79	84	86	87
400	75	80	89	91	94	95
500	80	84	91	95	97	98

Table 4. Comparison of Accuracy (%)

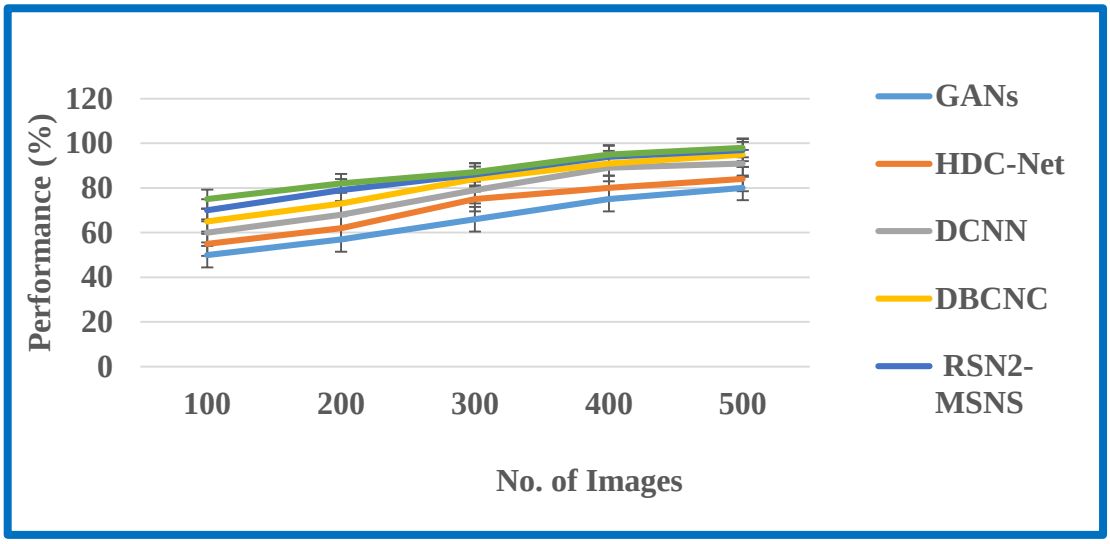

Figure 7: Comparison Chart for Accuracy

Table 4 and figure 7, the proposed DNRNN method achieves superior accuracy compared to GAN, HDC-Net, DCNN, DBCNC, and RSN^2-MSNS at all training set sizes. The accuracy gap is more significant for smaller training sets and narrows as more data is available, but DNRNN maintains its accuracy advantage even with 500 training images. DNRNN achieves the highest accuracy, with 1-6.7% improvement compared to the next best-performing RSN^2-MSNS with datasets ranging from 100 to 500.

4.4 False Score

The false positive (FP) pixels are those that the segmentation considers to be a part of the object but, in reality, they are not a part of it. On the other hand, the false negative (FN) pixels are those that are a part of the object but have been categorized as being outside of it by the segmentation.

Table 5. False Score (%)

No. of Images	GAN	HDC-Net	DCNN	DBCNC	RSN2-MSNS	DNRNN
100	36	34.2	31.1	28.4	25.1	22.5
200	41.1	39.2	36.2	30.1	27.1	25.8
300	45.2	40.2	41.3	32.4	30.2	29.2
400	50.2	49.2	47.4	34.6	31.1	30.5
500	50.2	50.8	45.8	33.5	32.5	30

.

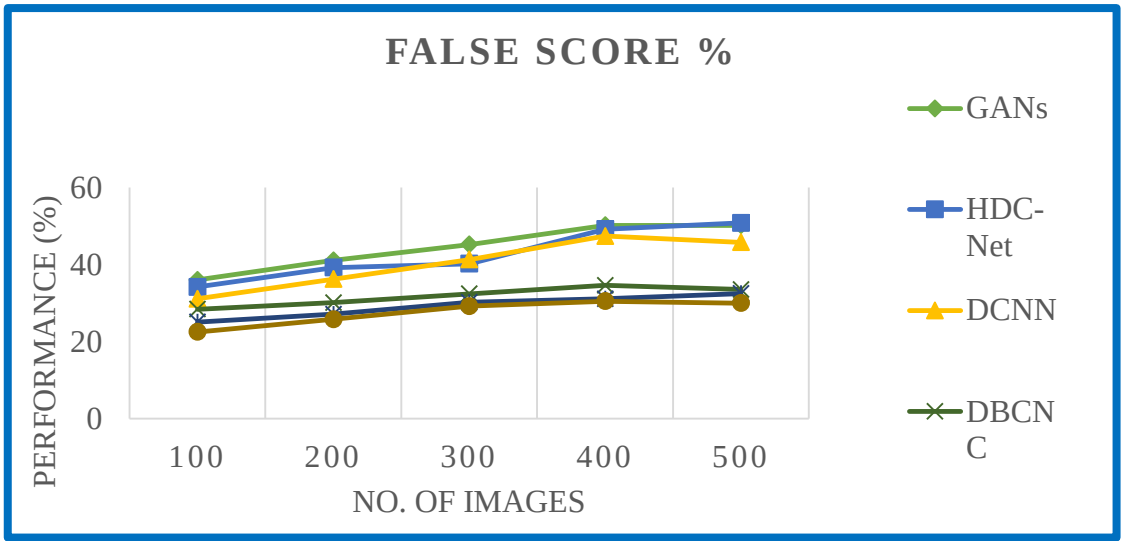

Figure 8. Comparison Chart for False Score

As shown in table 5 and figure 8, for 100 training images, DNRNN produces 22.5% false score, much lower than GAN (36%), HDC-Net (34.2%), DCNN (31.1%), DBCNC (28.4%), and RSN^2-MSNS (25.1%). As more training data is added, the gap between DNRNN and existing methods decreases slightly, but DNRNN maintains 8% advantage in false score reduction throughout. Finally, with 500 images, while GAN, HDC-Net, and DCNN have false scores clustered around 45-50%. DBCNC and RSN^2-MSNS have false scores of 33.5% and 32.5% respectively. DNRNN achieves a substantially better 30% false score, demonstrating the strength of its multi-scale capabilities.

CONCLUSION

The most prevalent use of MRI in the field of healthcare is specifically for the segmentation of tumors. Given the wide variety of content contained within medical images performs a vital role in the overall processing of image segmentation. The precise diagnosis of a brain tumor is necessary to devise the most effective treatment strategy, which can both treat the patient and extend their life. Fuzzy clustering, which can reliably anticipate tumor cells, is used in this work for tumor segmentation. Both traditional classifiers and the Dense-Net Recurrent Neuron Network (DNRNN) were used for classification during segmentation. The suggested method is found for feature extraction utilizing an effective model that was maintained. The features increased the concert of the classifier by improving Specificity, Sensitivity, Accuracy, False Score, and the ability to identify brain tumors. Results of the experiments demonstrate that our suggested strategy performs better and reaches a high accuracy.

REFERENCES

[1] ZainEldin H, Gamel SA, El-Kenawy EM, Alharbi AH, Khafaga DS, Ibrahim A, Talaat FM, “Brain Tumor Detection and Classification Using Deep Learning and Sine-Cosine Fitness Grey Wolf Optimization”, Bioengineering (Basel), Vol 10 issues 1, Article 18, 2022.

[2] Milica M. Badža, and Marko Č. Barjaktarović, “Classification of Brain Tumors from MRI Images Using a Convolutional Neural Network”, Applied Sciences, Vol 10 Issues 6, Article 1999, 2020.

[3] Muhtasim, D.A.; Pavel, M.I.; Tan, S.Y. "A Patch-Based CNN Built on the VGG-16 Architecture for Real-Time Facial Liveness Detection", Sustainability, Vol 14, Article 10024, 2022.
[4] S. Banerjee, S. Mitra, and B. U. Shankar, "Automated 3D segmentation of brain tumor using visual saliency " Information Sciences, Volume 424, ages 337-353, 2018.
[5] Rehman, M. A. Khan, T. Saba, Z. Mehmood, U. Tariq, and N. Ayesha, ''Microscopic brain tumor detection and classification using 3D CNN and feature selection architecture'', Microscopy Research & Technique, Vol 84 No 1, Pages 133–149, 2021.
[6] Hu and N. Razmjooy, ''Brain tumor diagnosis based on metaheuristics and deep learning,'' International Journal of Imaging System and Technology, Vol. 31, No. 2, Pages 657–659, 2021.
[7] Saba, A. S. Mohamed, M. El-Affendi, J. Amin, and M. Sharif, ''Brain tumor detection using fusion of handcrafted and deep learning features,'' Cognitive System. Research, Vol. 59, Pages 221–230, 2020.
[8] P. Kaur, G. Singh, and P. Kaur, ''Classification and validation of MRI brain tumor using optimised machine learning approach,'' ICDSMLA 2019, Proceedings of the 1st International Conference on Data Science, Machine Learning and Applications, Springer, Pages 172–189, 2020.
[9] T. Pandiselvi and R. Maheswaran, ''Efficient framework for identifying, locating, detecting and classifying MRI brain tumor in MRI images,'' Journal of Medical System, Vol. 43, No. 7, Pages 1–14, 2019.
[10] T. Zhou, S. Canu, P. Vera and S. Ruan, "Latent correlation representation learning for brain tumor segmentation with missing MRI modalities", IEEE Transactions on Image Processing, Vol 30, Pages 4263-4274, 2021.
[11] Guotai Wang, Wenqi Li, Sébastien Ourselin and Tom Vercauteren, "Automatic brain tumor segmentation based on cascaded convolutional neural networks with uncertainty estimation", Frontiers in Computational Neuroscience, Vol 13, 2019.
[12] Dingwen Zhang, Guohai Huang, Qiang Zhang, Jungong Han, Junwei Han, Yizhou Yu, "Cross-modality deep feature learning for brain tumor segmentation", Pattern Recognition, Volume 110, Article Number 107562, 2021.
[13] Zhengrong Luo, Zhongdao Jia, Zhimin Yuan, Jialin Peng, "HDC-Net: Hierarchical Decoupled Convolution Network for Brain Tumor Segmentation", IEEE J Biomed Health Inform, Vol 25 issues 3, Pages 737-745. 2021.
[14] A. Gumaei, M. M. Hassan, M. R. Hassan, A. Alelaiwi and G. Fortino, "A Hybrid Feature Extraction Method with Regularized Extreme Learning Machine for Brain Tumor Classification," IEEE Access, Vol. 7, Pages 36266-36273, 2019.
[15] Dingwen Zhang, Guohai Huang, Qiang Zhang, Jungong Han, Junwei Han, Yizhou Wang, "Exploring Task Structure for Brain Tumor Segmentation from Multi-Modality MR Images," in IEEE Transactions on Image Processing, Vol. 29, Pages 9032-9043, 2020.
[16] G. Manogaran, P. M. Shakeel, A. S. Hassanein, P. Malarvizhi Kumar and G. Chandra Babu, "Machine Learning Approach-Based Gamma Distribution for Brain Tumor Detection and Data Sample Imbalance Analysis," in IEEE Access, Vol. 7, Pages 12-19, 2019.
[17] M. S. Majib, M. M. Rahman, T. M. S. Sazzad, N. I. Khan and S. K. Dey, "VGG-SCNet: A VGG Net-Based Deep Learning Framework for Brain Tumor Detection on MRI Images," IEEE Access, Vol. 9, Pages 116942-116952, 2021.
[18] Y. Zhuang, H. Liu, E. Song and C. -C. Hung, "A 3D Cross-Modality Feature Interaction Network With Volumetric Feature Alignment for Brain Tumor and Tissue

Segmentation," in IEEE Journal of Biomedical and Health Informatics, Vol. 27, Number 1, Pages 75-86, 2023.

[19] M. A. Ottom, H. A. Rahman and I. D. Dinov, "Znet: Deep Learning Approach for 2D MRI Brain Tumor Segmentation," in IEEE Journal of Translational Engineering in Health and Medicine, Vol. 10, Pages. 1-8, 2022, Art no. 1800508.

[20] Y. Ding et al., "MVFusFra: A Multi-View Dynamic Fusion Framework for Multimodal Brain Tumor Segmentation," in IEEE Journal of Biomedical and Health Informatics, Vol. 26, Number 4, Pages 1570-1581, 2022.

[21] K. Muhammad, S. Khan, J. D. Ser and V. H. C. d. Albuquerque, "Deep Learning for Multigrade Brain Tumor Classification in Smart Healthcare Systems: A Prospective Survey," in IEEE Transactions on Neural Networks and Learning Systems, Vol. 32, Number 2, Pages 507-522, 2021.

[22] M. Ali, S. O. Gilani, A. Waris, K. Zafar, and M. Jamil, "Brain Tumor Image Segmentation Using Deep Networks," in IEEE Access, Vol. 8, Pages 153589-153598, 2020.

[23] T. A. Soomro et al., "Image Segmentation for MR Brain Tumor Detection Using Machine Learning: A Review," in IEEE Reviews in Biomedical Engineering, Vol. 16, Pages 70-90, 2023.

[24] Balasubramaniyan M, Navaneethan C, "Identifying peanut maturity based on Hyper Spectral Invariant Scaled Feature Selection using Adaptive Dense Net Recurrent Neural Network", Measurement: Sensors, Volume 24, Article Number 100500, 2022.

[25] P Priyanga & N C. Naveen, 2018. "Analysis of Machine Learning Algorithms in Health Care to Predict Heart Disease," International Journal of Healthcare Information Systems and Informatics (IJHISI), IGI Global, vol. 13(4), pages 82-97,2018.